Density functional theory calculation of the electronic structure of $Ba_{0.5}Sr_{0.5}TiO_3$: Photoluminescent properties and structural disorder

E. Longo,[1,*] E. Orhan,[2] F. M. Pontes,[1] C. D. Pinheiro,[1] E. R. Leite,[1] J. A. Varela,[2] P. S. Pizani,[3] T. M. Boschi,[3] F. Lanciotti, Jr.,[3] A. Beltrán,[4] and J. Andrés[4]

[1]*Departamento de Química, Universidade Federal de São Carlos, Caixa Postal 676, 13565-905, São Carlos, SP, Brazil*

[2]*Instituto de Química, Universidade Estadual Paulista, 14801-907, Araraquara, SP, Brazil*

[3]*Departamento de Física, Universidade Federal de São Carlos, Caixa Postal 676, 13565-905, São Carlos, SP, Brazil*

[4]*Departamento de Ciencies Experimentals, Universitat Jaume I, P.O. Box 6029 AP, 12080 Castello, Spain*

(Received 20 May 2003; revised manuscript received 7 August 2003; published 26 March 2004)

First-principles quantum-mechanical techniques, based on density functional theory (B3LYP level) were employed to study the electronic structure of ordered and deformed asymmetric models for $Ba_{0.5}Sr_{0.5}TiO_3$. Electronic properties are analyzed and the relevance of the present theoretical and experimental results on the photoluminescence behavior is discussed. The presence of localized electronic levels in the band gap, due to the symmetry break, would be responsible for the visible photoluminescence of the amorphous state at room temperature. Thin films were synthesized following a soft chemical processing. Their structure was confirmed by x-ray data and the corresponding photoluminescence properties measured.

DOI: 10.1103/PhysRevB.69.125115 PACS number(s): 71.15.Mb, 71.20.−b

I. INTRODUCTION

Our group recently demonstrated that amorphous titanates ($ATiO_3$, where A=Pb, Ca, Sr, and Ba), synthesized by a soft chemical process called the polymeric precursor method, displayed intense visible photoluminescence (PL) at room temperature.[1–3] We have reported several interesting properties of these amorphous titanates, including the fact that the PL emission wavelength depends on the exciting wavelength, suggesting electronic transitions between a distribution of vibronic states[4] and that the PL phenomena are related to the amorphous state.[2,5] These studies revealed important aspects. First, a simple water-based chemical process was used, allowing amorphous titanates to be processed at temperatures as low as 523 K in the form of thin films or particles. Second, theoretical and experimental results suggested that amorphous titanates are composed of a Ti–O network. The charge of the A cation must be compensated by negatively charged nonbridging oxygen (NBO) and the PL phenomenon is associated to this defect. The bond between the A cation and oxygen is basically ionic.

Among the compounds presenting PL properties, the perovskite-type semiconducting crystals with the chemical formula ABO_3 are well known.[6–8] For example, Eglitis *et al.*[9] demonstrated very recently through semiempirical quantum chemical calculations that the origin of the intrinsic excitonic (''green'') luminescence of ABO_3 perovskites at low temperature is linked to the recombination of electrons and hole polarons forming a charge transfer vibronic exciton (CTVE).

Over the last 10 years, renewed interest has been paid to the PL properties of titanates and especially of perovskite titanates such as $SrTiO_3$ and $BaTiO_3$.[10,11] Bouma and Blasse[12] reported that some crystalline titanates such as A_2TiOBO_4 (A=Li,Na; B=Si,Ge) show efficient PL at room temperature and some others only below room temperature ($LiTiOPO_4$ at 125 K, $BaTiO_3$ at 45 K, and Li_2TiO_3 at 250 K). They concluded that irregular titanate octahedra containing a short Ti–O distance show PL at room temperature if these octahedra are isolated from each other, and ascribed this effect to a broadening of the energy bands. More recently, several phenomena of PL at low temperature (45 K) have been reported for the $BaTiO_3$ crystal, and the observed effects have been correlated to the creation of CTVE[11] or to impurity centers, e.g., doping rare earth ions. When pure $SrTiO_3$ crystal samples are excited by radiation above their energy band gap, a broad luminescent band appears at low temperatures (35 K).[13–15]

The investigations about $SrTiO_3$ and $BaTiO_3$ crystals have been successfully extended to the electronic structures of impurities, surfaces, and defects.[16–18] Nowadays these conditions are known to play an important role in photoconductivity, PL, and others effects. Therefore, intense study about the electronic structures of the $SrTiO_3$ and $BaTiO_3$ compounds in the crystalline form has been carried out. For example, Saha *et al.*[19] have led a detailed study of the electronic structure and optical properties of paraelectric (cubic) $BaTiO_3$, using the tight-binding linearized muffin-tin orbital (TB-LMTO) method. The calculated values of the ground-state gap of paraelectric $BaTiO_3$ was 1.2 eV, much smaller than the experimental value of 3.4 eV.[20] The electronic structure of $SrTiO_3$ has been investigated by Mo *et al.*[21] using the first-principles orthogonalized linear combination of atomic orbitals (OLCAO) method, and a 1.45 eV gap has been found, smaller than the experimental gap reported to be 3.2 eV.[13] These underestimations of the gap values are inherent to the DFT methods. However, Heifets *et al.*[17] calculated a gap of 4.6 eV for $SrTiO_3$, in a better agreement with the experimental value using the hybrid B3PW functional.

Among the perovskite-type compounds, crystalline $Ba_xSr_{1-x}TiO_3$ in the powder and thin film forms, has been exhaustively investigated, owing to its high dielectric constant coupled with its good thermal stability. Shuvaeva *et al.*[22] have realized EXAFS measurements at the Ba K

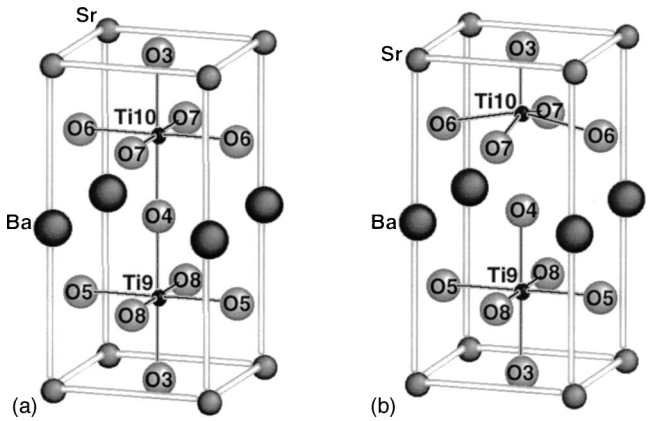

FIG. 1. The crystalline structure for symmetric BST-c (a) and asymmetric BST-a (b).

edge at room temperature, in $Ba_xSr_{1-x}TiO_3$ system. The results indicate that Ti atoms are disordered in a wide range of Sr concentration. Yuzyuk *et al.*[23] reported experimental evidence for the stress-induced tetragonal symmetry in a heteroepitaxial $Ba_{0.7}Sr_{0.3}TiO_3$ thin film on MgO (001) substrate. In addition, several studies have found interesting electrical properties in amorphous and crystalline $Ba_xSr_{1-x}TiO_3$ thin films prepared by physical or chemical processes.[24–28]

The dependence on so many different parameters makes interpretation of the results difficult: theoretical calculations can be helpful in this respect. In the present paper, we present a combination of laboratory experiments and high-level calculations into a synergetic strategy for identifying the origin of PL properties at room temperature in amorphous $Ba_xSr_{1-x}TiO_3$ system. It should allow us to demonstrate the fundamental role of structural disorder to generate PL emission in these materials. We choose for convenience to focus on the $Ba_{0.5}Sr_{0.5}TiO_3$ compound (BST) as a model for the $Ba_xSr_{1-x}TiO_3$ system. We use a $1\times1\times2$ supercell for representing the crystalline structure (BST-c) and a $1\times1\times2$ supercell in which the position of one titanium has been shifted by a (0 0 0.5 Å) vector to model a deformed asymmetric structure (BST-a), which stands for the amorphous phase of BST, as explained in Sec. III. Both structures are presented in Fig. 1.

The paper is organized as follows. In Sec. II the experimental methods of the BST thin films preparation are described, together with spectral measurement techniques. Section III presents the BST-c and BST-a structures, while Sec. IV gives the computational details. The results are discussed attempting to explain the PL phenomenon in Sec. V. Section VI resumes the main lines of our hypothesis of the origin of PL at room temperature in BST amorphous thin films.

II. COMPUTATIONAL DETAILS

The calculations were made within the framework of the density functional theory (DFT) using the gradient-corrected correlation functional by Lee, Yang, and Parr,[29] combined with the Becke3 exchange functional,[30] B3LYP, which has been demonstrated by Muscat *et al.* to be suitable for calculating structural parameters and band structures for a wide variety of solids.[31] The atomic centers have been described by all-electron basis sets 9763-311(d631)G for Ba, 976-41(d51)G for Sr, 86-411(d31)G for Ti, and 6-31G* for O.[32,33]

All the calculations were carried out with the crystalline orbital program CRYSTAL98.[34] The k-points sampling was chosen to be 40 points within the irreducible part of the Brillouin zone. The unit cell volume was optimized in an isotropic way. For simulating the displacement of the Ti atom, we used the ATOMDISP option provided with the CRYSTAL program.

The XCRYSDEN program was used to design the density of states and the band structure diagrams.[35]

III. EXPERIMENT

$Ba_{0.5}Sr_{0.5}TiO_3$ (BST) thin films studied in the present work were obtained from a soft chemical processing. Details of the preparation method can be found in the literature.[36] The polymeric precursor solution was spin-coated on substrates [Pt (140nm)/Ti (10nm)/SiO_2 (1000nm)/Si] by a commercial spinner operating at 6000 rev./min for 20 s (spin-coater KW-4B, Chemat Technology), via a Syringe filter to avoid particulate contamination. After spinning, the films were kept in ambient air at 423 K on a hot plate for 20 min to remove residual solvents. The heat treatment was carried out at 573 K in a tube furnace under oxygen flow, at a heating rate of 5 K/min, for different durations, to pyrolyze the organic materials. The BST thin films were structurally characterized using x-ray diffraction (XRD) (Cu Ka radiation). The diffraction patterns were recorded on a Siemens D5000 machine in a θ-2θ configuration, using a graphite monochromator. The spectral dependence of the optical absorbance of the crystalline and amorphous $Ba_{0.5}Sr_{0.5}TiO_3$ on quartz substrates was taken at room temperature in the total reflection mode, using Cary 5G equipment. The PL spectra of the BST thin films were taken with a U1000 Jobin-Yvon double monochromator coupled to a cooled GaAs photomultiplier and a conventional photon counting system. The 488.0 nm exciting wavelength of an argon ion laser was used, with the output power kept at 20 mW. A cylindrical lens was used to prevent the sample from overheating. The slit width was 100 μm. All the measurements were taken at room temperature.

IV. CRYSTAL STRUCTURE

BST crystallizes in the cubic perovskite-type structure (space group Pm3m, O_h symmetry). We built a $1\times1\times2$ supercell, whose fractional atomic positions are given in Table I. The strontium and barium atoms share the vertices of the unit cell; the titanium is at the center of the cube, surrounded by six oxygen atoms that occupy the middle of the faces, in a regular octahedral configuration [Fig. 1(a)]. The experimental and calculated values of the **a** parameter are, respectively, 3.951 and 3.901 Å. It results in ten atoms in the unit cell. Each Ti is surrounded by six O in an O_h configuration. This crystal structure will be called BST-c and can also be designed as $[TiO_6]$–$[TiO_6]$ (D_{4h}). It is worth mentioning

TABLE I. Atomic fractional coordinates of the $1\times1\times2$ BST supercell in the $P_{4/mmm}$ space group.

Atom	Position	x	y	z
Ba	1*a*	0	0	0
Sr	1*b*	0	0	0.5
O_3	1*c*	0.5	0.5	0
O_4	1*d*	0.5	0.5	0.5
O5 = O6 = O7 = O8	4*i*	0.5	0	0.25
Ti9 = Ti10	2*h*	0.5	0.5	0.25

that we checked all the presented results with the inversion of the Sr and Ba positions, without noting changes in the main facts.

XANES experimental results on the amorphous phase of $SrTiO_3$[37] and $PbTiO_3$[2] pointed out the coexistence of two types of environments for the titanium, namely, fivefold oxygen–titanium coordination ($[TiO_5]$ square-base pyramid) and sixfold oxygen–titanium coordination ($[TiO_6]$ octahedron). This certain degree of order in amorphous materials could be expected, since two or more atoms arranged close to each other in a stable configuration must necessarely have some degree of order because there always are minima of the potential energy. Furthermore, as it is well known, the details of the band structure in a solid are mainly determined by the potential within the unit cell, rather than by the long-range periodicity. This means that it is necessary to disturb the unit cell symmetry to disturb the energy band gap. Based on these results, we constructed another BST structure to represent the amorphous by shifting the titanium 10 by a (0 0 0.5 Å) vector, resulting in the fractional coordinates (0.5 0.5 0.814). This displacement turns the unit cell asymmetric, in which Ti10 is now surrounded by five oxygen atoms in a square-base pyramid conformation, while Ti9 stays in an octahedral environment. This asymmetric BST unit, BST-a, is the most simple model for representing the two titanium coordinations of the amorphous phase and can be designed as $[TiO_6]$–$[TiO_5]$ (C_{4v}) [see Fig. 1(b)].

V. RESULTS AND DISCUSSION

Figure 2 shows the evolution of the x-ray diffraction patterns of BST thin films prepared by the polymeric precursor method, deposited on platinum-coated silicon substrate and annealed at 573 K for 2, 4, and 8 h, and at 973 K for 2 h in an oxygen flow. A diffuse XRD pattern can be observed for the sample annealed at 573 K in the 2 to 8 h range, indicating the formation of an inorganic amorphous precursor after the pyrolysis process. The crystallization of BST in the cubic phase can be observed at 973 K. Figure 3 shows the PL spectra performed at room temperature for the thin films treated in an oxygen flow at 573 K and at 973 K for different amounts of time. A comparison of the different samples reveals that the PL behavior of the amorphous BST thin films is sensitive both to the thermal treatment history and to the duration of thermal treatment. As shown in the room-temperature PL spectra of Fig. 3, the intensity of PL increased with the time of heat treatment. However, BST thin

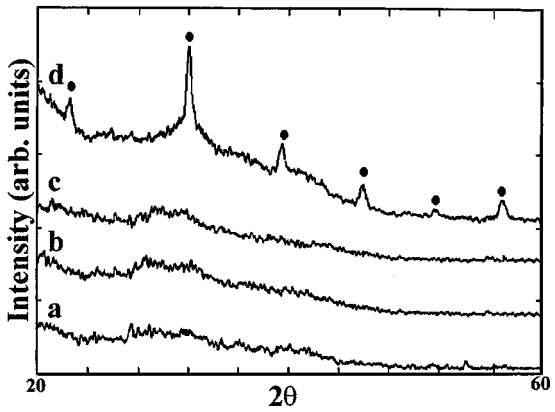

FIG. 2. X-ray patterns of BST thin films annealed at different temperatures and times. (a) 573 K/2 hours; (b) 573 K/4 hours; (c) 573 K/8 hours; and (d) 973 K/2 hours.

films annealed at higher temperatures (973 K), and thus crystalline as shown by the diffraction peaks of Fig. 2, showed no detectable PL response either at room temperature or at 10 K.

Figure 4 illustrates the spectral dependence of absorbance for the amorphous BST treated at 573 K for 8 h in an oxygen flow, and for the crystalline sample (treated at 973 K). Amorphous BST showed a spectral dependence on absorbance similar to that found in amorphous semiconductors such as amorphous silicon (Si) and insulators, while crystalline BST showed a typical interband transition of crystalline materials. These experimental results strongly indicate that in this case, the PL is directly related to the exponential optical edges and tails. The nature of these exponential optical edges and tails may be associated with localized defect states promoted by the disordered structure of the amorphous BST-a. The absorbance measurements, associated with the PL characterization of BST system, suggest a nonuniform band gap structure

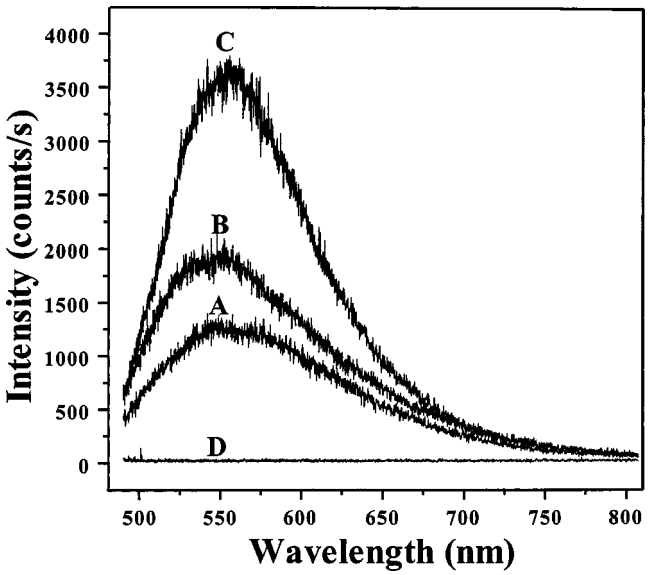

FIG. 3. Room temperature photoluminescence spectra of BST thin films heat treated at 573 K during (a) 2 hours; (b) 4 hours; (c) 8 hours; and (d) at 973 K during 2 hours.

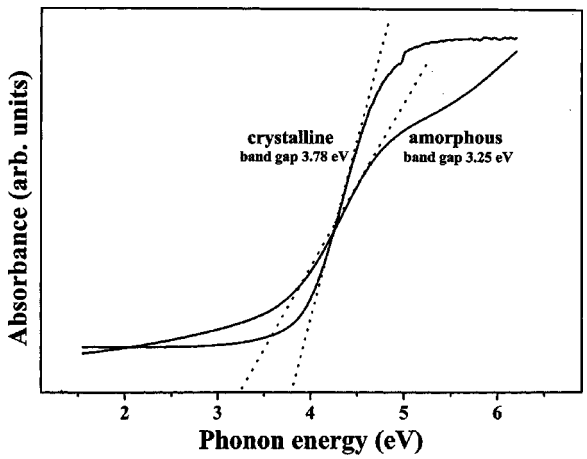

FIG. 4. UV-visible absorbance spectra for crystalline and amorphous BST thin films.

with a tail of localized states and mobile edges.

In order to understand the relationship between the structural disorder and the electronic defects that it generates, we performed a detailed theoretical study of the electronic structure in a crystalline (BST-c) and disordered (asymmetric) material (BST-a). To appreciate the difference in the electronic structure, it is convenient to make reference to quantities such as the band gap or the projected densities of states (DOS), which may be compared to each other, independently of the crystalline space group.

Figure 5(top) reports the calculated band structure of bulk BST-c. The top of the valence band (VB) is at the M point and is very close to the X point. The bottom of conduction band (CB) is at the Γ point. The minimal indirect gap between M and Γ is 3.78 eV, equal to the experimental one deduced from the observed optical absorption edge. The minimal direct gap at Γ is 3.89 eV.

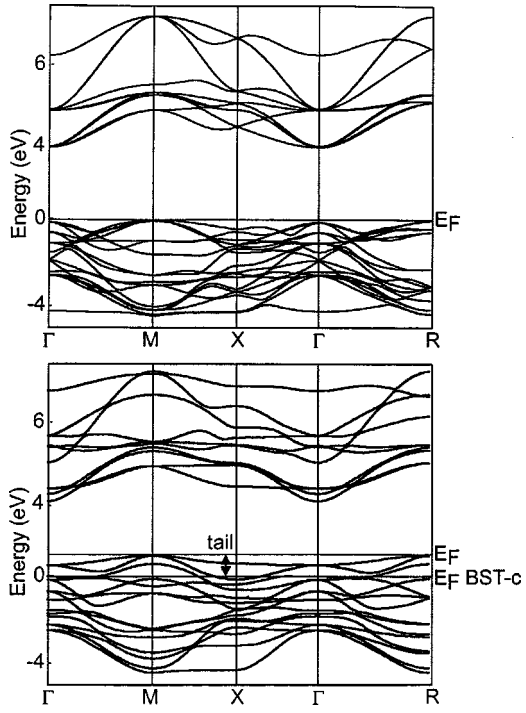

FIG. 5. The calculated energy band structure for BST-c (top) and BST-a (bottom). The zero of the energy scale was set at the Fermi energy of BST-c.

The calculated band structure of bulk BST-a is depicted in Fig. 5(bottom). The top of the VB is at the M point and the bottom of CB is at the Γ point, as in the case of BST-c. The indirect minimal gap between M and Γ is 3.06 eV, while the minimal direct gap at Γ is 3.75 eV. The indirect gap can be compared with the optical gap of the amorphous film that we found to be 3.25 eV.

These results show that our data are consistent with the interpretation that the exponential optical absorption edge and the optical band gap are controlled by the degree of disorder, structural and thermal, in the lattice of BST system (see Fig. 4).

For the BST-c [Fig. 5(top)], the valence bands are derived from O ($2p_x$, $2p_y$, $2p_z$) atomic orbitals, as well as from O ($3p_x$, $3p_y$, $3p_z$) polarization orbitals. They are separated by an indirect gap from the first conduction band, which derives from transition-metal titanium ($3d_{xy}$, $3d_{xz}$, and $3d_{yz}$) atomic orbitals, designated as "t_{2g}" by comparison with the [TiO_6] regular cluster (O_h). Above these six bands come four Ti ($3d_{z^2\text{-}y^2}$ and $3d_{z^2}$) character bands designated as "e_g." For the BST-a [Fig. 5(bottom)], although the VB is globally constituted of O ($2p_x$, $2p_y$, $2p_z$) and O ($3p_x$, $3p_y$, $3p_z$) character states, the top mainly depends on the oxygen located at the center of the structure, O4. The CB is composed of the $3d$ states of titanium, in an apparently random splitting of the bands.

For both BST-c and BST-a structures, the main contributions for each band are schematically represented as energy levels in Fig. 6. Each level symbolizes the eigenvalue of one band calculated at the Γ point. The dominating character of the bands at the Γ point is also indicated along the figures. The square modulus of minimum coefficient was set to 0.25. This scheme can be assimilated to the molecular orbital diagram of two linked titanium clusters: [TiO_6–TiO_6] in a D_{4h} geometry for BST-c and [TiO_6–TiO_5] in the C_{4v} geometry for BST-a. The top of the VB, globally O ($2p$) in the case of BST-c, is destabilized by the displacement of Ti10 and depends mainly on O4. By elongating the Ti10–O4 bond, we created new states located within the band gap of BST-c. This is in accordance with the absorbance tail observed for amorphous BST in Fig. 4. The Sr, Ba contribution to the VB is also shifted towards the highest energies and the Ba contribution becomes weak as the distance Ti10–Ba elongates. The bottom of the CB is also destabilized by the distortion, but in a minor way. Splitting of the Ti ($3d$) orbitals that was clearly "t_{2g}–e_g" in the case of BST-c becomes more confused. The apparition of a O4 ($2p$) contribution in the CB seems to indicate a reinforcement of the O4–Ti9 hybridization.

The calculated total and atom-resolved projected DOS of BST-c and BST-a structures are shown in Fig. 7, ranging from -9 eV below the top of the VB to 19 eV above. The upper VB is predominately made of the O ($2p$) states, equivalently distributed in the six oxygens of the structure.

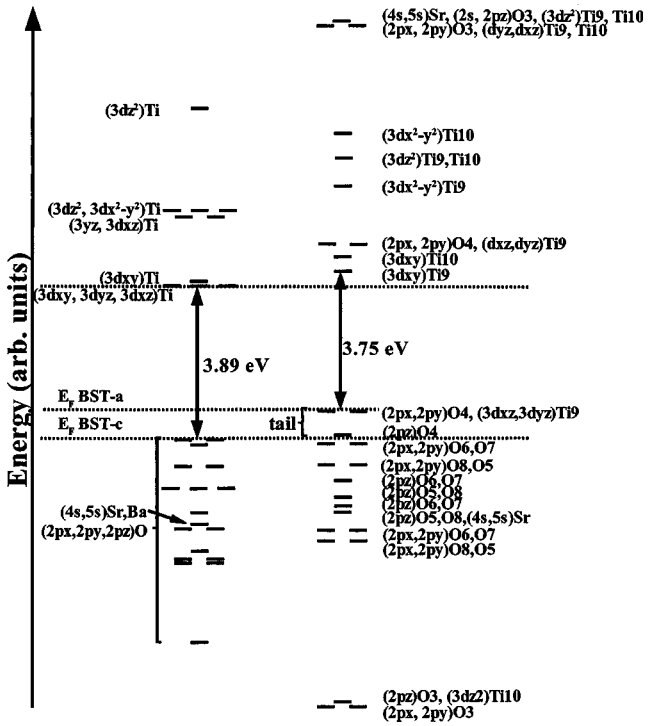

FIG. 6. Schematic diagram of the energy levels of the BST-c (left) and BST-a structure (right).

The CB is clearly made of the Ti $(3d)$ states. The Ti–O covalent bond creates a limited Ti $(3d)$ contribution in the O $(2p)$ region, as well as a weak O $(2p)$ contribution to the Ti $(3d)$ area. It has to be noted that this hybridization is more important in the case of BST-a than of BST-c. The Sr $(5s)$ states are out of the energy range, located around -17 eV. The Ba $(6s)$ states form a band above the Ti $(3d)$ states, from 15 to 16 eV. Their participation is more important in the case of the BST-c.

In order to further understand the electronic states in greater detail, we constructed contour and surface plots of the electronic charge density calculated in two selected planes for BST-c and BST-a. The first one is a vertical diagonal plane allowing one to see the Ba, Sr, Ti9, Ti10, O3, and O4 contributions [Fig. 8(a)]. The second one is a horizontal plane containing the Ti10, located at 3/4 of the cell edge for BST-c and at 0.814 for BST-a [Fig. 8(b)]. Figure 8(a) clearly shows that the bonding between Ba and $[TiO_6]$ is strongly ionic, as well as the bonding between Sr and $[TiO_6]$. From this figure, it is also obvious that substantial covalent bonding exists between Ti and O, due to the hybridization between the O $(2p)$ states and the Ti $(3d)$ states. Figure 8(b) also allows one to see the covalent nature of the Ti–O bond. It is visible that the covalent connection between Ti10 and O6/O7 is weaker in the case of BST-a.

The theoretical results indicate that the formation of a fivefold oxygen–titanium coordination $[TiO_5]$ through the displacement of Ti10 and the rupture of the Ti10–O4 bond introduces localized electronic levels with O4 $(2p_x, 2p_y, 2p_z)$ character above the VB of the structure before deformation [Fig. 7(bottom)]. The BST-c presents indeed a higher

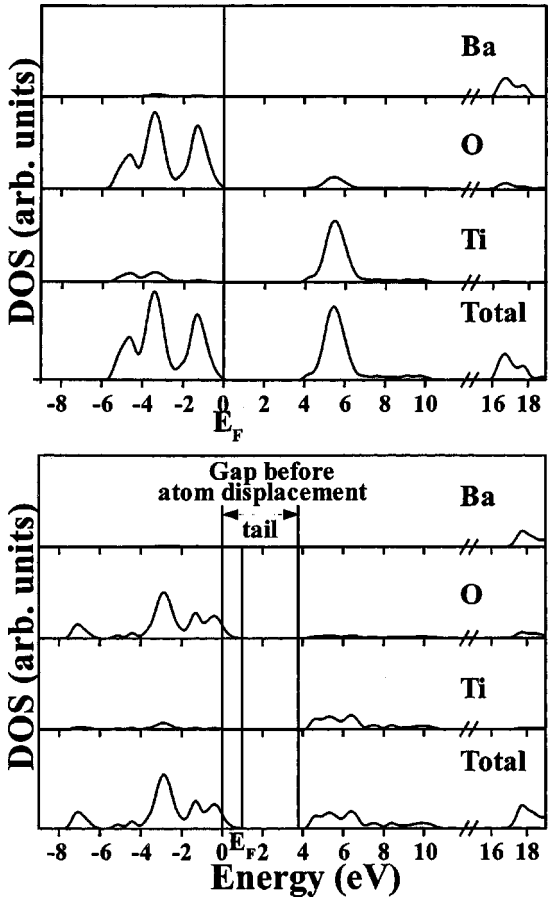

FIG. 7. The total and atom-projected density of states for BST-c (top) and BST-a (bottom). The zero of the energy scale was set at the Fermi energy of BST-c.

band gap than the BST-a, which is in agreement with experimental results observed by absorbance spectral data (Fig. 4). Moreover, it should be noticed here that the same calculations performed with progressive shifts of Ti10 along the **z** axis from $+0.1$ to $+0.9$ Å showed that the more localized Ti10, the smaller is the indirect gap. Therefore, a completely disordered model should have a much smaller gap, induced by the presence of localized levels in the band gap of the crystalline material.

The experimental PL measurements and UV-vis spectra indicate that the band structure of amorphous BST must contain localized levels that broaden the energy bands. This was confirmed by the calculations on a simple deformed crystal structure, BST-a, showing clearly the creation of those defect states.

VI. CONCLUSIONS

The photoluminescence at room temperature of $Ba_{0.5}Sr_{0.5}TiO_3$ (BST) was interpreted by means of first-principle calculations based on the density functional theory at B3LYP level, using a periodic supercell model. The electronic structures derived from the models proposed in this study for both crystalline (symmetric) and amorphous (asym-

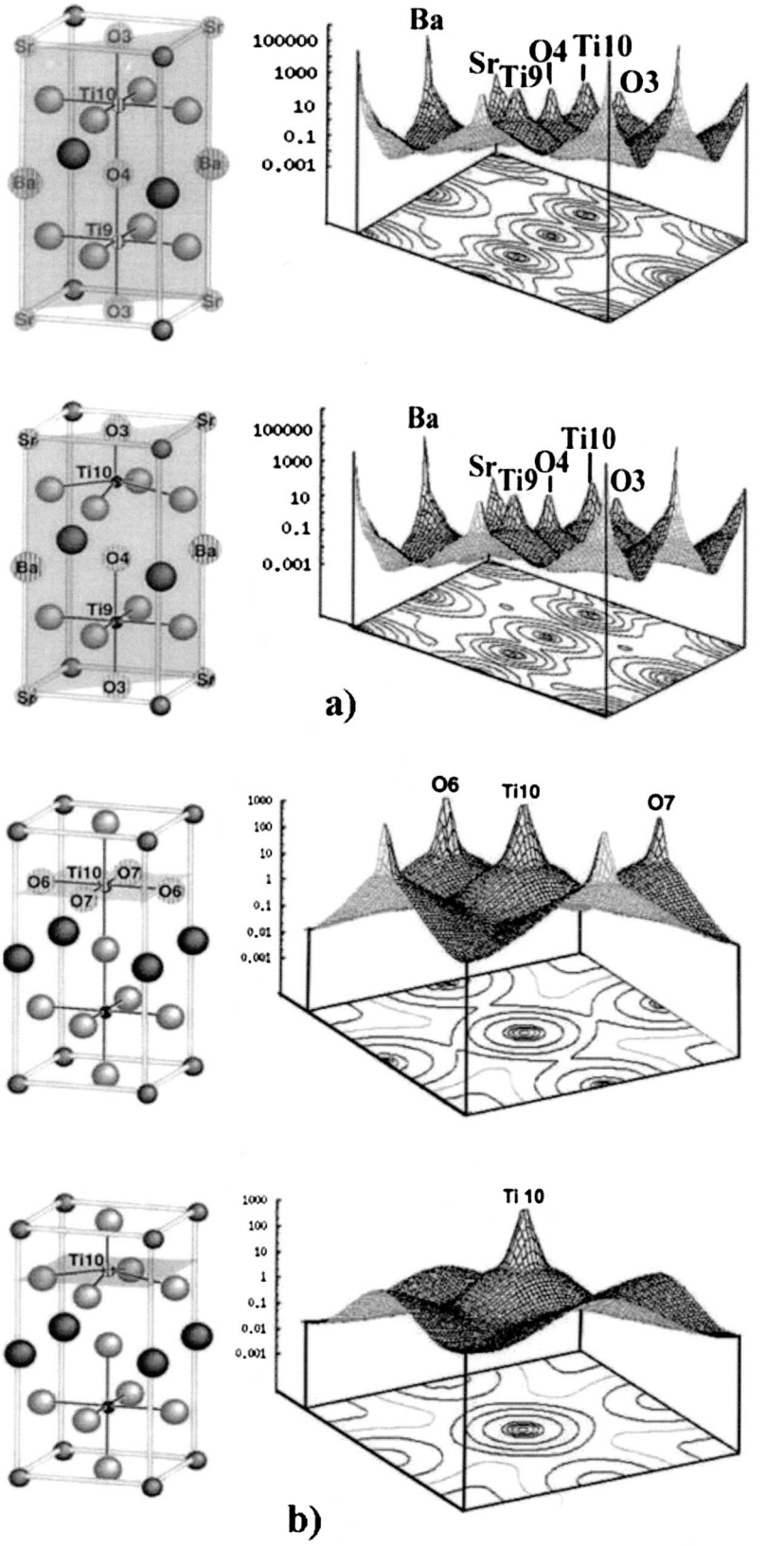

FIG. 8. The charge density contour and surface plots for crystalline and amorphous BST in two different planes: vertical diagonal plane (a) and horizontal plane cutting **z** axis at 0.75 for BST-c and at 0.814 for BST-a (b).

metric) structures allow one to calculate electronic energy band gap, as well as energy band structures that are consistent with experimentally determined optical band gap. Moreover, the foresight of localized electronic levels in asymmetric structure within the energy band gap of crystalline BST is in accordance with the experimental tail observed in the absorbance spectra of amorphous BST and with the dependence of the PL emission band on the excitation wavelength. Therefore, the localized electronic levels induced in the valence band by the symmetry break may be the reason for the

apparition of the visible photoluminescence emission in amorphous BST.

The knowledge of the geometric structure of BST provides an essential basis for understanding its photoluminescence behavior, and we think that this phenomenon is induced by the coexistence of both $[TiO_6]$ and $[TiO_5]$ connected configurations in the same crystal, allowing charge transfers from one cluster to another.

ACKNOWLEDGMENTS

This work was partially supported by the Brazilian research-financing institutions: Fundação de Amparo à Pesquisa do Estado de São Paulo-FAPESP/CEPID and Conselho Nacional de Desenvolvimento Científico e Tecnológico-CNPq/PRONEX.

*Electronic address: liec@dq.ufscar.br

[1] P.S. Pizani, E.R. Leite, F.M. Pontes, E.C. Paris, J.H. Rangel, E. Lee, E. Longo, P. Delega, and J.A. Varela, Appl. Phys. Lett. **77**, 824 (2000).

[2] E.R. Leite, F.M. Pontes, E.C. Paris, C.A. Paskocimas, E.J.H. Lee, E. Longo, P.S. Pizani, J.A. Varela, and V. Mastellaro, Adv. Mater. Opt. Electron. **10**, 235 (2000).

[3] E.R. Leite, F.M. Pontes, E.J.H. Lee, R. Aguiar, E. Longo, D.S.L. Pontes, M.S.J. Nunes, H.R. Macedo, P.S. Pizani, F. Lanciotti, Jr., T.M. Boschi, J.A. Varela, and C.A. Paskocimas, Appl. Phys. A: Mater. Sci. Process. **74**, 529 (2002).

[4] P.S. Pizani, H.C. Basso, F. Lanciotti, Jr., T.M. Boschi, F.M. Pontes, E. Longo, and E.R. Leite, Appl. Phys. Lett. **81**, 253 (2002).

[5] F.M. Pontes, E.R. Leite, E. Longo, J.A. Varela, P.S. Pizani, C.E.M. Campos, and F. Lanciotti, Adv. Mater. Opt. Electron. **10**, 81 (2000).

[6] R. Leonelli and J.L. Brebner, Solid State Commun. **54**, 505 (1985).

[7] J. Meng, Y. Huang, W. Zhang, Z. Du, Z. Zhu, and G. Zou, Phys. Lett. A **205**, 72 (1995).

[8] W.S. Cho and E. Hamada, J. Alloys Compd. **268**, 78 (1998).

[9] R.I. Eglitis, E.A. Kotomim, and G. Borstel, Eur. Phys. J. B **27**, 483 (2002).

[10] S. Eden, S. Kapphan, H. Hesse, V. Trepakov, V. Vikhnin, L. Jastrabik, and I. Gregora, Radiat. Eff. Defects Solids **149**, 107 (1999).

[11] R.I. Eglitis, E.A. Kotomim, and G. Borstel, J. Phys.: Condens. Matter **14**, 3735 (2002).

[12] B. Bouma and G. Blasse, J. Phys. Chem. Solids **56**, 261 (1995).

[13] M. Cardona, Phys. Rev. A **140**, 651 (1965).

[14] G.A. Barbosa, R.S. Katiyar, and S.P.S. Porto, J. Opt. Soc. Am. **68**, 610 (1978).

[15] C.N. Berglund and H.J. Braun, Phys. Rev. **164**, 790 (1967).

[16] H. Pinto and A. Stashans, Phys. Rev. B **65**, 134304 (2002).

[17] E. Heifets, R.I. Eglitis, E.A. Kotomin, J. Maier, and G. Borstel, Phys. Rev. B **64**, 235417 (2001).

[18] Ph. Ghosez, J.-P. Michenaud, and X. Gonze, Phys. Rev. B **58**, 6224 (1998).

[19] S. Saha, T.P. Sinha, and A. Mookerjee, Phys. Rev. B **62**, 8828 (2000).

[20] S.H. Wemple, Phys. Rev. B **2**, 2679 (1970).

[21] S.D. Mo, W.Y. Ching, M.F. Chisholm, and G. Duscher, Phys. Rev. B **60**, 2416 (1999).

[22] V. Shuvaeva, Y. Azuma, K. Yagi, H. Terauchi, R. Vedrinski, V. Komarov, and H. Kasatani, Phys. Rev. B **62**, 2969 (2000).

[23] Y.I. Yuzyuk, P. Simon, I.N. Zakharchenko, V.A. Alyoshin, and E.V. Sviridov, Phys. Rev. B **66**, 052103 (2002).

[24] E. Dien, J.-B. Briot, M. Lejeune, and A. Smith, J. Eur. Ceram. Soc. **19**, 1349 (1999).

[25] F.M. Pontes, E.R. Leite, D.S.L. Pontes, E. Longo, E.M.S. Santos, S. Mergulhão, P.S. Pizani, F. Lanciotti, Jr., T.M. Boschi, and J.A. Varela, J. Appl. Phys. **91**, 5972 (2002).

[26] F.M. Pontes, E.B. Araujo, E.R. Leite, J.A. Eiras, E. Longo, J.A. Varela, and M.A. Pereira-da-Silva, J. Mater. Res. **15**, 1176 (2000).

[27] J.D. Baniecki, R.B. Laibowitz, T.M. Shaw, K.L. Saenger, P.R. Duncombe, C. Cabral, D.E. Kotecki, H. Shen, J. Lian, and Q.Y. Ma, J. Eur. Ceram. Soc. **19**, 1457 (1999).

[28] W. Zhu, K. Tan, Q. Yan, and J.T. Oh, Sens. Actuators B **65**, 366 (2000).

[29] C. Lee, W. Yang, and R.G. Parr, Phys. Rev. B **37**, 785 (1988).

[30] A.D. Becke, J. Chem. Phys. **98**, 5648 (1993).

[31] J. Muscat, A. Wander, and N.M. Harrison, Chem. Phys. Lett. **42**, 397 (2001).

[32] http://www.tcm.phys.cam.ac.uk/~mdt26/crystal.html

[33] http://www.chimifm.unito.it/teorica/crystal/crystal.html

[34] V.R. Saunders, R. Dovesi, C. Roetti, M. Causa, N.M. Harrison, and C.M. Zicovich-Wilson, CRYSTAL98 *User's manual* (University of Torino, Torino, Italy, 1998).

[35] A. Kokalj, J. Mol. Graphics Modell. **17**, 176 (1999).

[36] F.M. Pontes, E. Longo, J.H. Rangel, M.I. Bernardi, E.R. Leite, and J.A. Varela, Mater. Lett. **43**, 249 (2000).

[37] F.M. Pontes, E. Longo, E.R. Leite, E.J.H. Lee, J.A. Varela, P.S. Pizani, C.E.M. Campos, F. Lanciotti, Jr., V. Mastellaro, and C.D. Pinheiro, Mater. Chem. Phys. **77**, 598 (2002).